

OPTICALLY PUMPED CESIUM-BEAM FREQUENCY STANDARD FOR GPS-III

R. Lutwak, D. Emmons, R. M. Garvey, and P. Vlitas
 Datum-Timing, Test & Measurement

Abstract

We describe an optically pumped cesium-beam frequency standard under development for deployment on the GPS-III satellite constellation. The objective of the project is to demonstrate the feasibility of a space qualified optically pumped cesium-beam frequency standard exhibiting a short-term stability of $\sigma_y(\tau) < 6 \times 10^{-12} \tau^{-1/2}$ with lifetime and reliability comparable to that of the current GPS-IIF cesium standards. In this paper, we report on the architecture and development progress of a prototype instrument that meets these goals with a minimal introduction of unproven technology. In particular, we discuss the design choices that have been made with particular emphasis on optical pumping and interrogation techniques, laser and optical technologies, and the realization of the prototype frequency standard. Preliminary performance data are presented.

INTRODUCTION

To date, cesium-beam frequency standards (CFS) deployed on the GPS satellites have met and exceeded the stability requirements necessary to achieve the timing and position accuracy of the GPS system. The user range error (URE) and timing error objectives for GPS-III have been laid out in the 1999 GPS System Operation Requirements Document (SORD). It has been shown that the technology currently being deployed for the GPS-IIF satellites meets the “Threshold” criterion established by the 1999 SORD, but not its “Objective” goal [1]. It is desirable to improve the stability of the CFS by a factor of two in order to accommodate the immediate and future needs of the GPS program.

The cesium frequency standards (CFS) currently being produced for use in GPS employ an atomic beam interrogation technique that has been in use for more than 30 years. Inhomogeneous magnetic fields are used for state selection and analysis and a hot-wire ionizer and electron multiplier are employed for signal detection. This technology is capable of supporting a frequency stability of order $\sigma_y = 2 \times 10^{-11} \tau^{-1/2}$ with an operating lifetime of 10 years. Since the principal noise mechanism in cesium-beam interrogation is the shot noise of the beam, achieving the desired twofold stability improvement would incur an unacceptable fourfold reduction in life for the cesium-beam tube due to cesium exhaustion and related life-limiting effects. The introduction of optical pumping and detection techniques to the CFS permits more efficient utilization of the atomic beam and, thus, improved stability without reduction of lifetime.

The stability of any passively interrogated atomic frequency standard is given by

$$\sigma_y \approx \frac{FWHM}{(S/N)\sqrt{Hz}} \times \frac{1}{\nu_0} \quad (1)$$

where

$FWHM$ is the Full-Width at Half-Maximum of the resonance line,
 $(S/N)\sqrt{Hz}$ is the Signal/Noise of the detected signal measured in a 1 Hz bandwidth,

and

v_0 is the atomic resonance frequency.

In a cesium-beam standard, the Fourier transform limit of the resonance linewidth is determined by the atom-microwave interaction time and, thus, is proportional to $1/L$, where L is the distance between the two zones of the Ramsey cavity. Under optimal conditions, the signal/noise is limited by the shot noise of the atomic beam, i.e. $(S/N)_{\sqrt{\text{Hz}}} \propto \sqrt{I_{\text{ATOM}}}$, where I_{ATOM} is the atomic beam flux, which falls off (approximately) as the square of the distance from the oven aperture, r . Then, $(S/N)_{\sqrt{\text{Hz}}} \propto \sqrt{1/r^2} = 1/r$, and insofar as r/L is similar across designs, the stability of a cesium-beam frequency standard is independent of its size.

Extensive laboratory research on the physics and performance of optically pumped cesium frequency standards (OPCFS) was conducted in the 1990s, notably the development of primary standards at the National Institute of Standards and Technology (NIST) in Boulder, CO [2], and in Paris at the Laboratoire Primare du Temps et des Fréquences (LPTF) [3] and the Laboratoire de l'Horloge Atomique (LHA) [4]. Though these efforts were generally directed towards frequency *accuracy*, rather than *stability*, the two are related by the need to make accurate measurements in a timely fashion and, as such, this body of research provides the theoretical and experimental foundation for our development effort. Typically, the experimental OPCFS have demonstrated stability on the order of $\sigma_y = 3 - 5 \times 10^{-12} \tau^{-1/2}$ which, along with the scaling law of Equation (1), provides confidence that a compact OPCFS can achieve the stability goals of this project.

The objective of this effort is the development of an S-Class, radiation-hardened OPCFS, designated Datum 4430, with frequency stability $\sigma_y = 6 \times 10^{-12} \tau^{-1/2}$ and lifetime of 10 years.

PROJECT STRATEGY

Our organization is currently producing the Datum Model 4410 S-Class CFS for the GPS-IIF program. The 4410, which completed qualification in 2000, is the first microprocessor-controlled frequency standard qualified for use in the GPS space segment. In addition to microprocessor control, the 4410 incorporates other features typically found on high-performance commercial cesium-beam frequency standards, including a 48-bit direct digital synthesizer (DDS) and a sophisticated RF system. The microprocessor allows for sophisticated lock acquisition and servo algorithms, as well as supporting comprehensive state-of-health monitoring and telemetry. The overall architecture of the optically pumped CFS is quite similar to that of the conventional (4410) CFS and we are able to incorporate significant subsystems from the 4410 into the 4430 OPCFS with minimal modification.

The 4410, with its cover removed, is shown on the left of Figure 1, below. The base is built in two layers: the “lower deck” contains the power supplies, in intimate thermal contact with the satellite chassis, and the “upper deck” contains the microprocessor-based servo board, analog and digital signal paths, and DDS. On the upper level, the Datum Model 7610 beam tube is mounted in the foreground, supported by elastomer shock mounts. Behind the beam tube, a vertical housing contains the RF electronics, with the exception of the quartz oscillator, frequency multiplier, and 9.2 GHz SAW oscillator, which are mounted on its backside.

The 4430 OPC is shown on the right-hand side of the Figure 1. The power supplies, servo board, RF

systems are taken directly from the 4410 with minimal modification. The chassis footprint is unchanged, but is allowed to grow vertically by 2 inches to accommodate the physics package (including the optical bench) and an additional 25 in² of printed circuit board inside the vertical housing for additional electronics to support the optical system. In addition to the 2" height increase, the weight and power consumption are increased by 5 pounds and 5 watts, respectively.

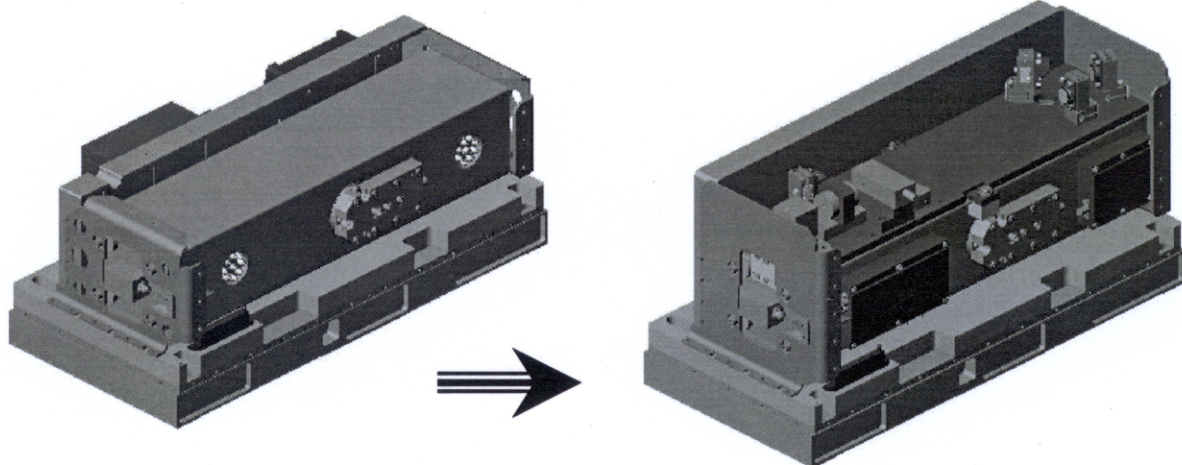


Figure 1: Evolutionary path from 4410 CFS to 4430 OPCFS

Adopting the mechanical and electronic design of the 4410 allows us to focus our engineering efforts on the physics package. Aside from the physics package, the 4430 requires only a half-dozen or so electronic components that have not been previously qualified on the 4410.

PHYSICS PACKAGE

The design of the physics package for the 4430 OPCFS involves numerous tradeoffs between performance and the size, weight, and reliability of the instrument. Wherever possible, our design has given preference to existing technologies and techniques and proven components.

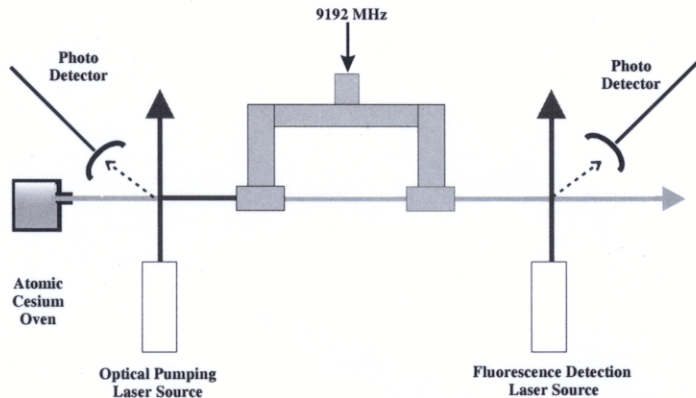


Figure 2: Schematic of OPC physics package

The principal components of the optically pumped cesium physics package are illustrated diagrammatically

in Figure 2. The oven produces a collimated beam of cesium atoms directed along the principal axis of the beam tube. The beam passes through three distinct regions, hereafter denoted as state preparation, microwave interrogation, and state detection regions. Each of the three regions is magnetically shielded and contains provision for application of uniform magnetic field. In the state preparation and detection regions, laser beams intercept the atomic beam at right angles. The light scattered from the atomic beam is collected on a silicon photodiode detector internal to the CBT vacuum jacket. In the state preparation region, the laser beam induces optical pumping transitions, depleting one of the two ground state hyperfine levels. In the microwave interrogation region, a conventional Ramsey-type microwave resonator induces transitions to repopulate the vacant level. Finally, in the state detection region, resonance fluorescence is used to measure the extent of the repopulation. In operation, the detected signal is used to servo the microwave local oscillator to the cesium ground state hyperfine frequency.

OPTICAL SCHEME

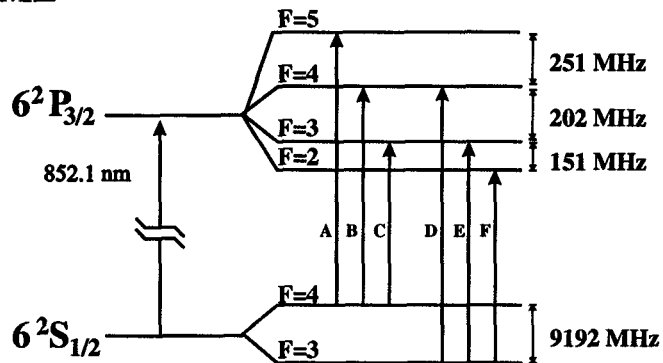


Figure 3: Relevant energy levels of the cesium D₂ manifold

A simplified energy level diagram for cesium is shown in Figure 3. Only the $^2\text{P}_{3/2}$ excited state is shown along with the $^2\text{S}_{1/2}$ ground state. The transitions between these states correspond to the D₂ resonance lines with wavelengths near 852 nm. There are six allowed optical transitions between the ground and excited states, labeled A-F in Figure 3. These transitions fall into two classes. The transitions labeled A and F are the so-called “cycling” transitions, because they drive atomic transitions to excited states that principally decay only to the originating ground state. The light scattering process, thus, cannot efficiently induce transitions between the ground states. The transitions B-E are referred to as “pumping transitions,” because they drive transitions to excited states which are coupled to both ground states. Light tuned to the B or C transitions depletes the upper ground state, while the D or E transitions deplete the lower ground state.

Using a single laser for optical pumping, tuned to an optimal pumping transition, e.g. transition B, the resulting $F=3$ population is roughly evenly distributed among the seven Zeeman sublevels ($m_F = -3, -2, \dots, 2, 3$), leaving about 13% of the atoms in the desired $m_F=0$ clock state. The addition of a second “repumping” laser, to deplete all of the $F=3, m_F \neq 0$ states, e.g. transition E, allows 100% pumping to the $m_F=0$ clock state.

For optical detection of the final state, we may choose between the pumping transitions, B-E, or the cycling transitions, A, F. If a pumping transition is used for detection, e.g. transition B, each atom scatters only a couple of photons before optically pumping into a “dark” ($F=4$) state. Limitations of photon

collection and detector efficiency result in sub-unity atom detection efficiency. In this case the overall $(S/N)_{\sqrt{Hz}}$ is limited by the shot noise of the photocurrent in the detector, rather than by the flux-limited shot noise of the atomic beam [5]. If instead a cycling transition, e.g. transition A, is used for detection, each atom scatters about 50 photons during its flight time across the laser beam, guaranteeing 100% detection efficiency and $(S/N)_{\sqrt{Hz}}$ limited principally by the atomic beam shot noise. These considerations are summarized in the following table:

Table 1: Relative efficiencies of laser schemes

Number of Colors	Pumping Transition	Detection Transition	Pumping Efficiency	Detection Efficiency	Overall Efficiency
One	B	B	13 %	$\approx 20\%$	3%
Two	B	A	13 %	100%	13%
Three	B, E	A	100%	100%	100%

Experimentally, we and others have found that the single laser scheme, with overall efficiency of 3%, yields system performance that is only marginally superior to that of a conventional (magnetically selected) CBT, but that the two-color scheme is capable of achieving short-term stability, $\sigma_y < 5 \times 10^{-12} \tau^{-1/2}$.

For the 4430 OPCBT, we have selected a two-color scheme, using the $|^2 S_{1/2}, F=4\rangle \rightarrow |^2 P_{3/2}, F=4\rangle$ transition for state preparation (pumping transition B) and the $|^2 S_{1/2}, F=4\rangle \rightarrow |^2 P_{3/2}, F=5\rangle$ transition for detection (cycling transition A). This combination of transitions provides the highest efficiency of all two-color schemes [6]. Moreover, because the two colors are separated by only 250 MHz, both beams can be generated from a single laser source, using an acousto-optic modulator (AOM) to generate the second color. The addition of a third color, in order to fully complete the pumping process, would require unacceptable compromise of complexity, reliability, size, and weight, requiring an additional laser source, offset by 9.2 GHz, as well as additional servos and transmissive polarizing optics.

OPTICAL SYSTEM

The 4430 optical system is shown schematically in Figure 4, below.

The key components of the physics package include a single laser source that produces 2 mW of laser power at the cycling transition, A. The beam passes through a TeO₂ acousto-optic modulator (AOM), which is driven by the output of a quartz oscillator at 251.4 MHz. Two beams emerge from the AOM, the original cycling beam and a second beam, of about 150 μ W, red-detuned by 251.4 MHz to the B pumping transition. The emergent beams are spatially separated by a deviation angle of 50 mRad and free-space optics are used to separately direct the two beams into the cesium-beam tube. The fluorescence signal from the optical pumping region is used to servo the laser frequency to the cesium resonance.

Figure 5 shows the optical layout of the physics package including, from lower right to upper left, the laser source, optical isolator, and AOM. Two folding mirrors in each laser beam emerging from the AOM permit precision alignment relative to the atomic beam through windows in the vacuum jacket.

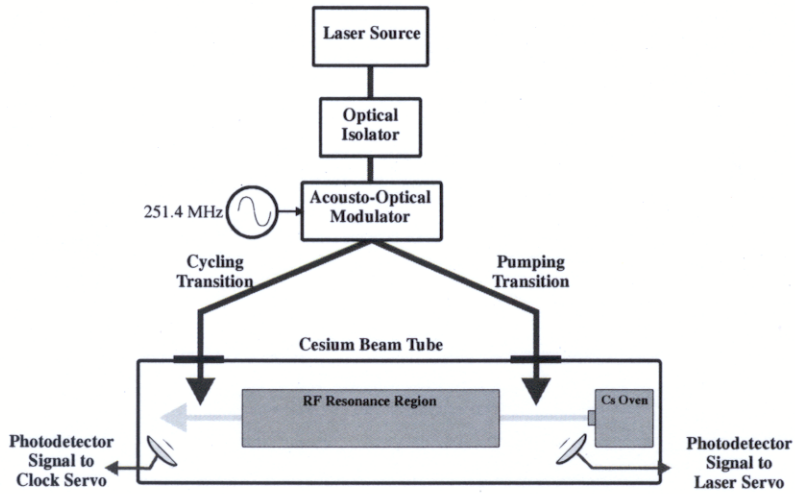


Figure 4: Block diagram of 4430 physics package

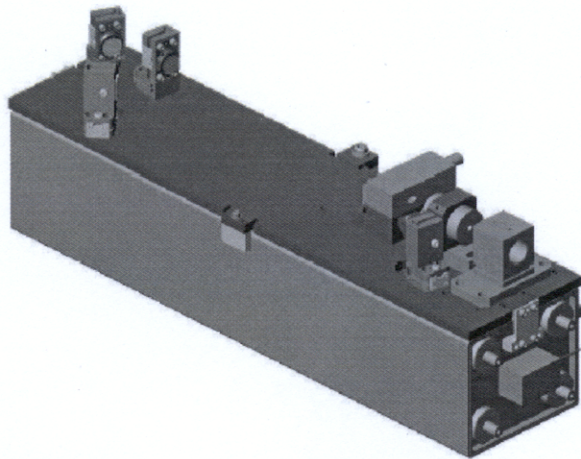


Figure 5: 4430 physics package assembly

CESIUM-BEAM TUBE

The cesium-beam tube for the OPCFS has evolved from the Datum Model 7610 CBT, which is currently deployed in the 4410 CFS. The state-selecting magnets, hot-wire ionizer, and electron multiplier have been deleted and replaced by the optical collection regions. Otherwise, the RF resonance region, the cesium-beam oven, and most of the details of the assembly and vacuum integrity are essentially unchanged.

OPTICAL BENCH

The thermal and mechanical stability of the optical system, and its alignment to the cesium beam are critical to the overall performance of the OPCFS. The performance can be predicted by evaluating the relative alignment of the laser beams to the atomic beam at each of the two ports in response to environmental perturbations. This alignment is complicated by several factors, including the registration of the internal CBT components to the exterior of the vacuum jacket, thermal distortions of the system in response to changing ambient conditions, and additional distortions due to release of gravity and pressure in on-orbit operation. There is necessarily a thermal mismatch between the stainless steel CBT vacuum jacket and the optical bench, which must be manufactured of lightweight aluminum.

The optical bench was designed by first determining experimentally the instrumental sensitivity to misalignments. Then the influence of misalignment due to each component was determined by optical ray tracing. A comprehensive thermomechanical model was built of the entire instrument, including both internal and ambient thermal sources, and finite-element analysis was performed to determine the thermoelastic response of the mechanical systems in response to environmental perturbations. Finally, the relative misalignment of the lasers to the atomic beam was determined based on the sensitivities computed earlier. The entire process was repeated iteratively throughout the design of the optical bench and component holders.

As shown in Figure 5, the bench is rigidly mounted near to the midpoint of the beam tube and allowed to expand, via flexures along its principal length. Additional flexures machined into the optical bench itself, prevent buckling in response to distortions of the beam tube jacket. Thermoelastic modeling has shown that this design will meet the performance requirements of this project throughout an ambient operating range of 0-50°C, as well as under the perturbations due to gravity and pressure release.

PHYSICS PACKAGE PERFORMANCE

In the early stages of this development effort, the physics package occupied most of the area of a 4'x 8' laboratory optical table, the electronic systems were adapted from those of a commercial cesium frequency standard, and several different laser sources were evaluated. The electronic and software design has proceeded in parallel with the physics package engineering, and we have developed a clear understanding of the influence of laser performance on that of the OPCFS. The performance data presented in this section were obtained using the physics package discussed in the previous section, mated to the electronics from a commercial (Datum Model 4310) cesium standard. The laser source for these data was a commercial external-cavity diode laser (ECDL).

We find that, at cesium oven temperatures consistent with a 10-year lifetime limited by cesium exhaustion, the instrument performance is limited principally by the shot-noise of the atomic beam. Figure 6, below, shows the optical fluorescence signal, measured at the downstream collection region, as the RF frequency is swept 1 MHz across the central resonance feature at 9192631770 Hz.

Figure 6 shows the microwave spectrum of the OPC physics package including all seven of the $\Delta m=0$ magnetic hyperfine transitions between the F=3 and F=4 ground states. The centermost “clock” transition, $|F = 3, m_F = 0\rangle \rightarrow |F = 4, m_F = 0\rangle$, is shown in greater detail in Figure 7, below.

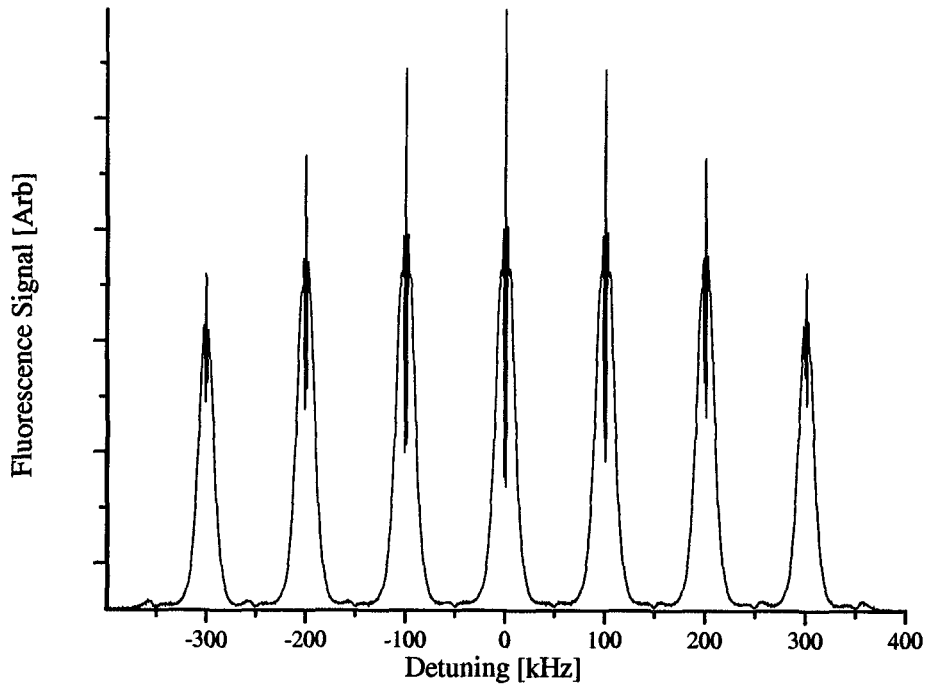


Figure 6: RF resonance spectrum across all ground state $\Delta m=0$ transitions

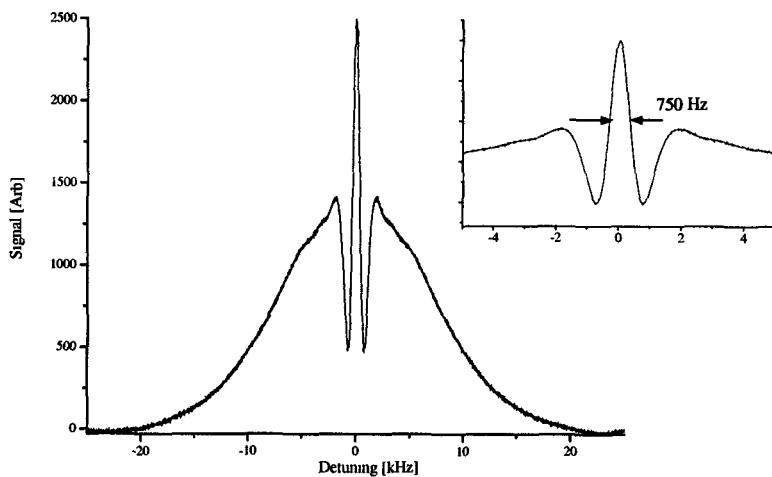


Figure 7: Clock transition resonance. Inset shows detail of central fringe

Figure 7 shows the central resonance feature from Figure 6, above, with the inset showing the detail of the central Ramsey resonance. The linewidth of the central resonance is about 750 Hz and the $(S/N)\sqrt{Hz} \approx 30,000$, measured at the half-max interrogation points on the Ramsey line. From Equation 1, this predicts a short-term stability of $\sigma_y \approx 3 \times 10^{-12} \tau^{-1/2}$. Incorporating this physics package with the commercial electronics testbed, we have measured the Allan deviation of the OPCFS.

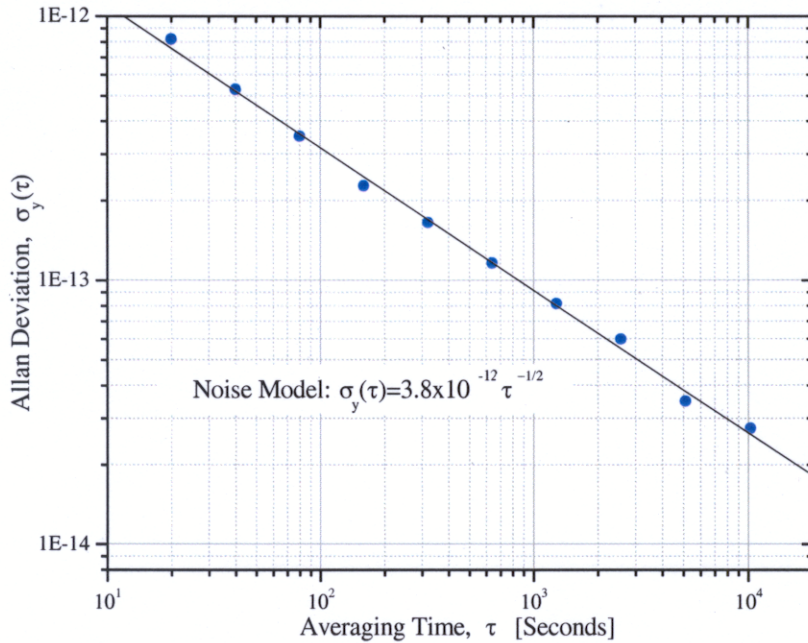


Figure 8: Allan deviation of physics package in commercial testbed

Figure 8 shows the Allan deviation of the physics package, utilizing the commercial electronics testbed, pumped by a commercial external cavity laser, and operating at an oven temperature consistent with a 10-year mission life. Also shown is a white frequency noise model fit to short-term stability given by $\sigma_y = 3.8 \times 10^{-12} \tau^{-1/2}$, in good agreement with the prediction of Equation 1 and the goals of this project.

ULTIMATE PERFORMANCE LIMITS

In a conventional, magnetically selected, CFS, the short-term stability can be arbitrarily improved by increasing the cesium beam flux (oven temperature) at the expense of lifetime reduction. Because the $(S/N)_{\sqrt{Hz}}$ improves only as the square root of the atomic beam flux, this leads to the familiar relationship that $\sigma_y \propto T_{life}^{-1/2}$, i.e. a twofold improvement in STS requires a fourfold reduction in lifetime. This relationship only holds true insofar as other noise sources in the system are negligible compared to the atomic beam shot noise. In the OPCFS, we are confronted with a slightly different scenario, in part because the laser source contributes noise that is comparable to that of the shot noise of the atomic beam and partly due to the overall improved performance of the OPCFS that operates in a regime where other noise sources, negligible in the conventional instrument, become increasingly significant. The most significant contributing noise sources are summarized in this section.

ATOMIC BEAM SHOT NOISE

Based on first-principles calculations of atomic beam flux and optical pumping and detection efficiency,

we estimate that the short-term stability limit, due solely to shot noise in the atomic beam, is roughly

$$\begin{aligned}\sigma_y^{\text{Atoms}} &\approx 3 \times 10^{-12} \tau^{-1/2} @ \text{Low Flux (10 yr. life)} \\ &\approx 1 \times 10^{-12} \tau^{-1/2} @ \text{High Flux (3 yr. life)}\end{aligned}$$

where the “Low Flux” and “High Flux” conditions set the scale of attainable performance with reasonable lifetime.

LASER FREQUENCY NOISE

Figure 9, below, illustrates the effect of laser frequency noise on the fluorescence signal.

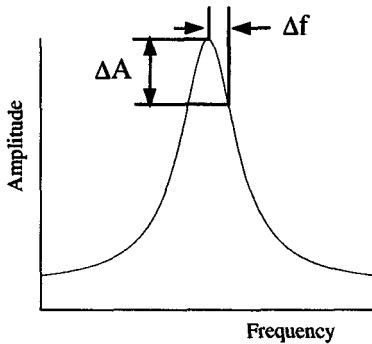


Figure 9: Effect of laser frequency noise on detected signal

The Lorentzian lineshape in Figure 9 represents the resonance fluorescence line for the detection process. Small frequency excursions of the laser (Δf) result in amplitude deviations (ΔA) of the detected signal. Note that the detected deviations are indistinguishable from atomic shot noise.

Typically, frequency noise on laser sources is characterized by the laser linewidth, which is the integral of laser frequency fluctuations over the bandwidth from infinity to the reciprocal integration time of the measurement system. In our case, we are principally interested in noise contributions in a relatively narrow bandwidth (typically 1 Hz) at frequencies which are even multiples of the interrogation frequency (typically several tens of Hz). As such, independent measurements of the time-averaged linewidth, do not necessarily provide the necessary criteria for determining the OPCFS performance. Ideally, one must consider the broadband power spectrum of the laser frequency to determine clock performance.

Moreover, because the atomic lineshape is Lorentzian, the spectral transformation from the incident light to the scattered spectrum is nonlinear. The scattering process effectively mixes noise from all frequencies into the detection bandwidth. Complete understanding of the mixing process and subsequent prediction of the clock performance from the independent analysis of the laser source requires not only a linear measurement of the laser's frequency and amplitude power spectrum, but also a complete theoretical model of the laser-atom interaction, including all possible states and transitions. Such an analysis is underway at Aerospace Corporation [7], but is beyond the scope of this paper.

We have evaluated several laser sources for this program, including both commercial and homemade external-cavity diode lasers (ECDL), Distributed Bragg Reflector (DBR) lasers, Vertical Cavity Surface Emitting Lasers (VCSEL), and conventional cleaved-facet diode lasers. In general, we have found a

monotonic relationship between the specified linewidth of the device and the measured $(S/N)_{\sqrt{Hz}}$, though it is difficult to quantify the relationship. One technique which we have used to evaluate lasers is to measure the $(S/N)_{\sqrt{Hz}}$ of the fluorescence signal, scattering from an atomic beam of extraordinarily high flux. This sets a limit on the maximum $(S/N)_{\sqrt{Hz}}$ that can be achieved in a shot-noise-limited beam. Typically, we find that conventional and DBR-type lasers are capable of supporting $(S/N)_{\sqrt{Hz}}$ up to about 10,000 and commercial ECDL lasers support up to $(S/N)_{\sqrt{Hz}} \approx 75,000$. Using a homemade ECDL, under optimum conditions, we have observed $(S/N)_{\sqrt{Hz}} \approx 150,000$.

PHOTODETECTOR AND PRE-AMPLIFIER NOISE

The level of the photocurrent detected at the fluorescence photodetector is typically 10 nA. This sets a limit on the allowable additive noise due to the intrinsic noise of the photodetector as well as the first stage of the transimpedance amplifier. There are many components that contribute to the overall noise figure of the detector system, which is dominated by the photon shot noise on the detector ($\phi_{shot} \approx 550\text{nV}/\sqrt{\text{Hz}}$) and the Johnson (thermal) noise of the transimpedance resistor ($\phi_{Johnson} \approx 400\text{nV}/\sqrt{\text{Hz}}$). Overall, assuming uncorrelated noise sources, the noise contribution of the detection system $\phi_{Total} = \sqrt{\phi_{shot}^2 + \phi_{Johnson}^2 + \dots} \approx 700\text{nV}/\sqrt{\text{Hz}}$, which limits the $(S/N)_{\sqrt{Hz}} \approx 140,000$.

OCXO PHASE NOISE

Audoin [8,9] has shown the theoretical limitations to frequency stability imposed by intermodulation effects, first pointed out for pulsed interrogation by Dick [10]. Phase noise of the OCXO at frequencies that are even harmonics of the modulation (interrogation) rate contribute to limit the short-term stability of the OPCFS. Spectral frequency noise components, around even harmonics of the modulation of the interrogating oscillator, are translated (aliased) into the frequency control loop. For white phase noise,

$$\sigma_y(\tau) = 0.45\sqrt{S_y(2f_m)}\tau^{-1/2}.$$

The oscillator in the 4410 CFS, Datum model 9400 exhibits $L(2f_m) = -139\text{dBc}$ at 10.23 MHz, which leads to $S_y(2f_m) = 10^{-24}$ at 9.2 GHz and an ultimate limit on stability of $\sigma_y(\tau) \approx 5 \times 10^{-13}\tau^{-1/2}$.

SUMMARY OF PERFORMANCE LIMITATIONS

The performance limitations discussed in this section are summarized in Table 2. Given that the noise sources summarized in the table are uncorrelated, the overall performance limit is given by their quadrature sum,

$$\sigma_y = \sqrt{(\sigma_y^{\text{Atoms}})^2 + (\sigma_y^{\text{Laser}})^2 + (\sigma_y^{\text{PreAmp}})^2 + \dots} > 1.5 \times 10^{-12}.$$

Table 2: Ultimate limits to OPCFS performance

Effect	Stability Limit
Atom Beam Shot Noise	$\sigma_y^{\text{Atoms}} \approx 3 \times 10^{-12} \tau^{-1/2}$ @ Low Flux (10 yr. life) $\approx 1 \times 10^{-12} \tau^{-1/2}$ @ High Flux (3 yr. life)
Laser Frequency Noise	$\sigma_y^{\text{Laser}} \approx 4 \times 10^{-12} \tau^{-1/2}$ w/DBR laser $\approx 1 \times 10^{-12} \tau^{-1/2}$ w/ECDL
Photodetector/Pre-amplifier	$\sigma_y^{\text{PreAmp}} \approx 5 \times 10^{-13} \tau^{-1/2}$
OCXO	$\sigma_y^{\text{OCXO}} \approx 5 \times 10^{-13} \tau^{-1/2}$

Testing the ultimate performance of the instrument is essential, not only to verify our understanding of the limitations discussed above, but also because operating at optimum performance provides rapid and accurate measurement of systematic and environmental effects.

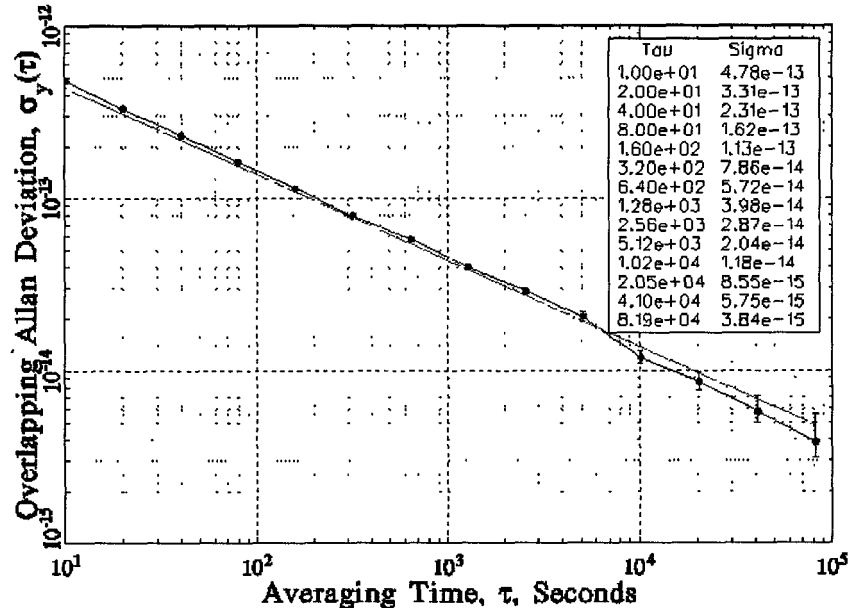


Figure 10: OPCFS operating in high-performance configuration

Figure 10 shows the Allan deviation for the OPCFS operating at high oven-flux and pumped by an ECDL source. These data represent 10 days of unattended operation. The model fit shown represents a white-frequency noise model corresponding to $\sigma_y(\tau) = 1.4 \times 10^{-12} \tau^{-1/2}$.

CONCLUSIONS

We have described the development of an S-class optically pumped cesium-beam frequency standard for the GPS-III program. We have outlined our project goals and strategy, which emphasize reliability and evolution from proven technologies to the maximum extent possible. We have nearly completed the development of a prototype physics package, which demonstrates short-term stability of $\sigma_y(\tau) \approx 4 \times 10^{-12} \tau^{-1/2}$, under operating conditions consistent with a 10-year instrument lifetime. In the upcoming phase of the project, our engineering efforts will focus on the development of a suitable laser source, as well as the integration of the physics package into the electronic and mechanical configuration of the instrument.

ACKNOWLEDGMENTS

The authors gratefully acknowledge financial support for this project by the Naval Research Laboratory Contract number N00173-00-C-2049.

We also acknowledge the following individuals for providing valuable technical and theoretical support:

Jim Camparo – *Aerospace Corporation*

Marc Daigle, Bill Bell, and Peter Hadfield – *Topsfield Engineering Services*

Hayward Merritt, John Parker, and Dwayne Taylor – *Datum – Timing, Test & Measurement*

REFERENCES

- [1] A. Wu and B. Feess, 2001, “*Development and Evaluation of GPS Space Clocks for GPS III and Beyond*,” in Proceedings of the 32nd Annual Precise Time and Time Interval (PTTI) Systems and Applications Meeting, 28-30 November 2000, Reston, Virginia, USA (U.S. Naval Observatory, Washington, DC), pp. 331-340.
- [2] See, for example, R .E. Drullinger, J. P. Lowe, D. J. Glaze, and J. Shirley, 1993, “*NIST-7, the New US Primary Frequency Standard*,” in Proceedings of the 1993 IEEE International Frequency Control Symposium, 2-4 June 1993, Salt Lake City, Utah, USA (IEEE Publication 93CH3244-1), pp. 71-74.
- [3] See, for example, E. de Clercq, G. D. Rovera, S. Bouzid, and A. Clairon, 1993, “*The LPTF Optically Pumped Primary Frequency Standard*,” *IEEE Transactions on Instrumentation and Measurement*, IM-42, 457-461.
- [4] See, for example, B .Boussert, *et al.*, 1997, “*Frequency Evaluation of a Miniature Optically Pumped Cesium Beam Clock*,” in Proceedings of the 11th European Frequency and Time Forum (EFTF), 4-6 March 1997, Neuchâtel, Switzerland, pp. 58-62.
- [5] J.Vanier and C.Audoin, 1989, *The Quantum Physics of Atomic Frequency Standards* (IOP Publishing,Ltd., Bristol, England), p. 765 ff.
- [6] G.Avila, *et al.*, 1987, “*State selection in a cesium beam by laser-diode optical pumping*,” *Physical Review*, A36, 3719-3727.
- [7] J. Camparo, 2002, “*Influence of Laser Noise on the Optically Pumped, Atomic-Beam Clock*,” in these

Proceedings.

- [8] C. Audoin, V. Candelier, and N. Dimarcq, 1991, “*A Limit to the Frequency Stability of Passive Frequency Standards Due to an Intermodulation Effect*,” **IEEE Transactions on Instrumentation and Measurement**, **IM-40**, 121-125.
- [9] R. Bariellet, V. Giordano, J. Viennet, and C. Audoin, 1992, “*Microwave Interrogation Frequency Noise and Clock Frequency Stability: Experimental Results*,” in Proceedings of the 6th European Frequency and Time Forum (EFTF), 17-19 March 1992, Noorwijk, Netherlands, pp. 453-456.
- [10] G. J. Dick, 1988, “*Local Oscillator Induced Instabilities in Trapped Ion Frequency Standards*,” in Proceedings of the 19th Annual Precise Time and Time Interval (PTTI) Applications and Planning Meeting, 1-3 December 1987, Redondo Beach, California, USA, pp. 133-147.